JGR Space Physics

RESEARCH ARTICLE
10.1029/2023JA032176

Multi-Instrument Observations of the Evolution of Polar Cap Patches Associated With Flow Shears and Particle Precipitation

Duan Zhang[1,2], Qing-He Zhang[1,3], Kjellmar Oksavik[2,4], Zan-Yang Xing[1], L. R. Lyons[5], Hui-Gen Yang[1,6], Guo-Jun Li[7], Keisuke Hosokawa[8], Atsuki Shinbori[9], Yu-Zhang Ma[1], Yong Wang[1], and Xiang-Yu Wang[1]

[1]Shandong Provincial Key Laboratory of Optical Astronomy and Solar-Terrestrial Environment, Institute of Space Sciences, Shandong University, Weihai, China, [2]Department of Physics and Technology, University of Bergen, Bergen, Norway, [3]State Key Laboratory of Space Weather, Center for Space Science and Applied Research, Chinese Academy of Sciences, Beijing, China, [4]Arctic Geophysics, University Centre in Svalbard, Longyearbyen, Norway, [5]Department of Atmospheric and Oceanic Sciences, University of California, Los Angeles, CA, USA, [6]Polar Research Institute of China, Shanghai, China, [7]Lab BLOS Reliable Informat Transmiss, Chongqing University Posts & Telecommun, Chongqing, China, [8]Department of Communication Engineering and Informatics, University of Electro-Communications, Chofu, Japan, [9]Institute for Space-Earth Environmental Research (ISEE), Nagoya University, Nagoya, Japan

Key Points:

- Cold dense plasma in the polar cap can appear either via transport of solar extreme ultraviolet plasma or after a hot patch cools down
- Soft-electron precipitation and flow shears both influence the Tongue of Ionization restructuring and the appearance of polar cap patches
- The enhanced plasma density is reduced due to decreased production and transport of cold nightside low-density plasma

Supporting Information:

Supporting Information may be found in the online version of this article.

Correspondence to:

Q.-H. Zhang,
zhangqinghe@sdu.edu.cn

Citation:

Zhang, D., Zhang, Q.-H., Oksavik, K., Xing, Z.-Y., Lyons, L. R., Yang, H.-G., et al. (2023). Multi-instrument observations of the evolution of polar cap patches associated with flow shears and particle precipitation. *Journal of Geophysical Research: Space Physics*, *128*, e2023JA032176. https://doi.org/10.1029/2023JA032176

Received 18 OCT 2023
Accepted 21 NOV 2023

Abstract Simultaneous observations from Defense Meteorological Satellite Program, Swarm, Resolute Bay all-sky imagers, GPS Total Electron Content and Super Dual Auroral Radar Network, are used to investigate the evolution and key characteristics of the Tongue of Ionization (TOI) being restructured into a polar cap patch. Six satellites crossed the TOI of patch as it moved from the dayside to the nightside. It was initially hot, then a mix of both cold and hot, and finally it became a cold patch. This suggests that cold patch is not only a result of solar extreme ultraviolet radiation, but may also develop when a hot patch cools down. Soft-electron precipitation and flow shears both contribute to the TOI restructuring and the appearance of polar cap patch. The plasma density of patch at ~500 km was at least 4 times higher than at ~800 km. The plasma density enhancement gradually decreased as the patch evolved due to decreased production and transport of cold nightside low-density plasma. Moreover, the duskward motion of the patch was influenced by changes in the ionospheric convection pattern.

Plain Language Summary The appearance of high-density plasma is a common phenomenon in the polar ionosphere. High-density polar cap patches usually form near the dayside sunlit region, and then move from the dayside to the nightside with the ionospheric flow. In the paper, we use multiple instruments including six satellites and ground-based observations to carefully investigate an event that started out on the dayside. It was initially a hot tongue of ionization (TOI) of high density and high electron temperature, followed by a mix of hot and cold (high vs. low electron temperature), before it finally became a cold patch. Soft-electron precipitation and flow shears both influenced the dayside high-density TOI plasma restructuring and the appearance of polar cap patch. The enhanced plasma density gradually weakened as the plasma migrated toward the nightside due to decreased production and transport of cold nightside low-density plasma. Moreover, the duskward motion of the patch was influenced by changes in the ionospheric convection pattern.

1. Introduction

The polar cap patch is a common source of irregularities in the polar ionosphere, associated with transient dayside magnetopause reconnection (e.g., Carlson et al., 2004; Lockwood & Carlson, 1992). A polar cap patch consists of high-density F region ionospheric plasma at least twice as dense as the background, ranging from ~100 to 1,000 km (e.g., Crowley, 1996; Moen et al., 2008). The density profile of the patch varies with altitude and usually maximizes at ~300 km (e.g., Ma et al., 2023; Nishimura et al., 2021; Zhang et al., 2011). Ren et al. (2018) used the Resolute Bay Incoherent Radar to report that patches have significantly different plasma characteristics at different altitudes and in different magnetic local time (MLT) sectors.

Enhanced electron density is often found at mid-latitudes during geomagnetic storms, where it is known as a storm enhancement density (SED). The SED can penetrate deep into the cusp and polar cap, where it is called

a Tongue of Ionization (TOI). The SED/TOI may be further segmented into patches in the dynamic cusp region in association with variable convection and magnetopause reconnection (e.g., Goodwin et al., 2015; Zhang et al., 2011, 2013a). Then, the patches are transported from the dayside to the nightside along the ionospheric convection pattern (e.g., Dungey, 1961; Oksavik et al., 2010; Zhang, Zhang, Lockwood, et al., 2013, 2015, 2020; D. Zhang et al., 2021). Strong electron density gradients and small-scale density structures can occur at the edges of patches, which may result in strong scintillation of trans-ionospheric signals (e.g., Aarons, 1982; Basu et al., 1987; Mitchell et al., 2005; Moen et al., 2013). Kivanç and Heelis (1997) suggested that the small-scale density structures power is slightly higher on the patches trailing edge. Therefore, an improved understanding of the evolution and key characteristics of polar cap patches is of great importance for the space weather community, with ultimate benefits for society as well.

Polar cap patches are divided into two categories using the ion/electron temperature (Ti/Te) (e.g., Ma, Zhang, Xing, Heelis, et al., 2018; Zhang et al., 2017). Cold patches (high density and lower electron temperature, Ti/Tc > 0.8) are associated with the ionization by solar extreme ultraviolet (EUV) radiation at mid-latitude, and hot patches (high density and higher electron temperature, Ti/Te < 0.8) are associated with particle precipitation. The cold patches are related to solar activity and found in the central polar cap (D. Zhang et al., 2021, 2022). The hot patches are found close to the auroral oval, associated with strong auroral emissions, ion upflows, and flow shears (e.g., Lorentzen et al., 2010; Ma et al., 2023; Nishimura et al., 2014; Zhang et al., 2023). The electron temperature of a hot patch may decrease to the same level as the ion temperature when the particle precipitation decreases, that is, it becomes a cold patch (Ma et al., 2023), which was obtained by analyzing two different patch events, rather than a complete evolution process of a patch.

In this paper, we use concurrent in situ observations from Defense Meteorological Satellite Program (DMSP) satellites and Swarm satellites, and ground observations from the red line all-sky imager (ASI) at Resolute Bay (RSB), GPS Total Electron Content (GPS TEC) and the Super Dual Auroral Radar Network (SuperDARN) to reveal the evolution and key characteristics at different altitudes of a TOI/patch. We suggest that a cold patch may evolve from structuring in the hot TOI, and discuss the significance of soft-electron precipitation and flow shears on polar cap patch evolution, as well as the relationship between patch and dayside auroral arcs. The high-density TOI plasma was initially hot, followed by a mix of cold and hot, and finally it became a cold patch. Six satellites crossed the event as it moved from the dayside to the nightside, offering widespread in situ observations.

2. Data Sources

The DMSP satellites fly in polar-orbits at ~840 km altitude with 101-min orbital period. Key instruments are the Precipitating Electron and Ion Spectrometer (Special Sensor for Precipitating particles, Version 5 (SSJ/5)) (Hardy et al., 2008), Special Sensor for Ions, Electrons and Scintillation (SSIES) (Greenspan et al., 1986), and the Special Sensor Ultraviolet Spectrographic (SSUSI) instrument (Paxton et al., 1992). The SSJ/5 provides the energy fluxes of electrons and ions in 19 energy channels from 32 eV to 30 keV. The SSIES offers the plasma densities, temperature, and ion drift velocities. The SSUSI measures far-ultraviolet emissions from 115 to 180 nm, and the Lyman-Birge-Hopfield short (LBHS) band (~140–150 nm) observations are used here.

The Swarm mission consists of three satellites in polar orbits with 93 min orbital period. Swarm-A and C are in ~460 km altitude, and Swarm-B is in ~520 km altitude. The Langmuir probe electron density data with 0.5 s resolution (Buchert et al., 2015) are used here.

The RSB ASIs are ground-based all-sky imagers at RSB (74.8°N, 264.9°E). These ASIs capture images at multiple wavelengths such as 557.7 and 630.0 nm (e.g., Shiokawa et al., 1999, 2009). The 630.0 nm (assumed emission height of ~250 km) ASI is used to monitor the aurora, and images are obtained every 2 min with an exposure time of 30 s.

SuperDARN is a network of ground-based, high-frequency (HF) radars for detecting the upper atmosphere and ionosphere from mid to polar latitudes in the Northern and Southern Hemispheres (Chisham et al., 2007). Each radar measures the line-of-sight component of the $\mathbf{E} \times \mathbf{B}$ drift velocity of ionospheric irregularities, which are fitted into maps of the ionospheric convection pattern.

The Total Electron Content (TEC) data are usually obtained by using the differential delays of multiple transmitted frequencies from satellites of a Global Navigation Satellite System. Here we used processed TEC data from

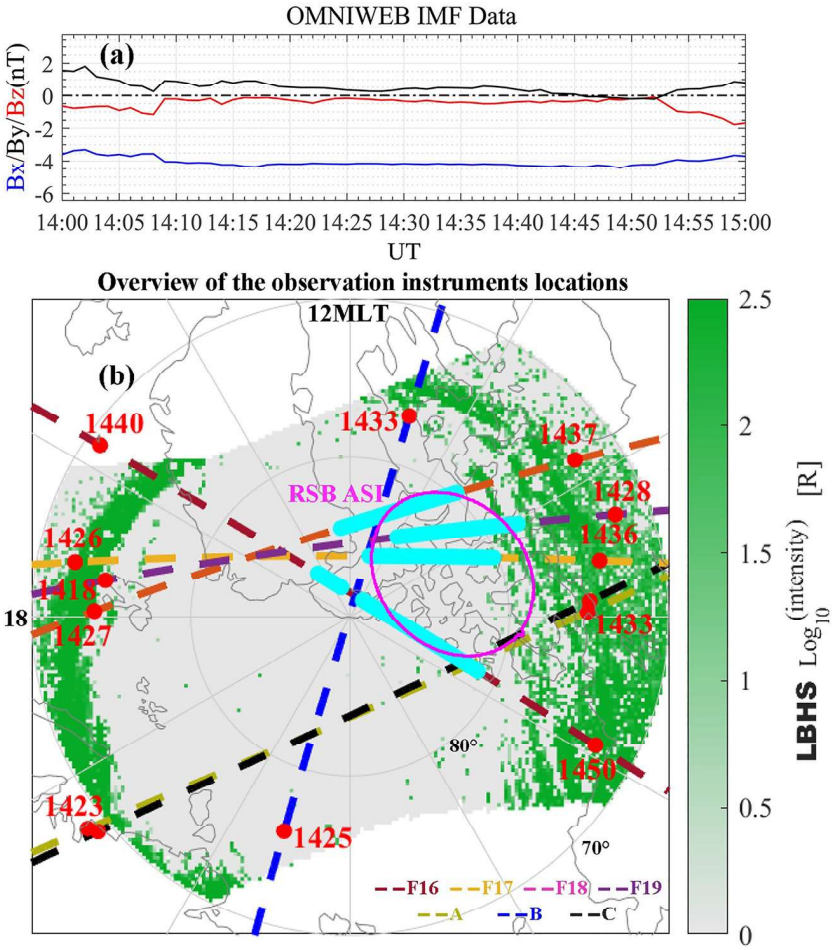

Figure 1. (a) The interplanetary magnetic fields (IMF) conditions during 1400–1500 UT on 12 December 2015 using a 7-min time delay. (b) An overview of the observation instruments ranges. The tracks of Defense Meteorological Satellite Program (DMSP) F16-F19 and Swarm A-C are superimposed on top of the DMSP F17 and F18 Special Sensor Ultraviolet Spectrographic auroral observations at 1425–1438 UT. The cyan-blue lines mark the location of observed plasma density enhancement. The magenta circle highlights the field-of-view of the 630.0 nm all-sky imager at Resolute Bay.

the Madrigal database. The TEC data's spatial resolution is 1° in latitude by 1° in longitude grid with 5-min time resolution.

3. Observation

Concurrent observations from four DMSP (F16-F19) satellites, three Swarm (A-C) satellites, RSB ASI, GPS TEC and SuperDARN were used to analyze the evolution and key characteristics of a high-density TOI/patch at 1420–1450 UT on 12 December 2015. Figure 1a shows the interplanetary magnetic fields (IMF) B_x, B_y, B_z in Geocentric Solar Magnetic coordinates using a 7-min time delay for 1400–1500 UT on 12 December 2015. The time delay consists of 5 min for solar wind propagation from the bow shock to the subsolar magnetopause, and 2 min from the subsolar magnetopause to the dayside ionosphere (Liou et al., 1998; Xing et al., 2012). During this period, IMF remained strongly radial (negative B_x) with very small positive B_y and negative B_z. The solar wind velocity varied between 510 and 550 km/s, and the solar wind density varied between 2 and 3.7 cm^{-3} (not shown). Figure 1b gives an overview of the tracks of DMSP F16-F19 and Swarm A-C over the polar region superimposed on the top of the DMSP F17 and F18 SSUSI auroral observations for 1425–1438 UT. The cyan-blue lines mark the location of the observed plasma density enhancement along each orbit. The magenta circle highlights the field-of-view with the zenith angle less than 70° of the 630.0 nm ASI at RSB. The DMSP F16-F19 and Swarm A-C flew over the polar region within half an hour (crossing order: F19, Swarm-A/B/C, F17, F18, and F16),

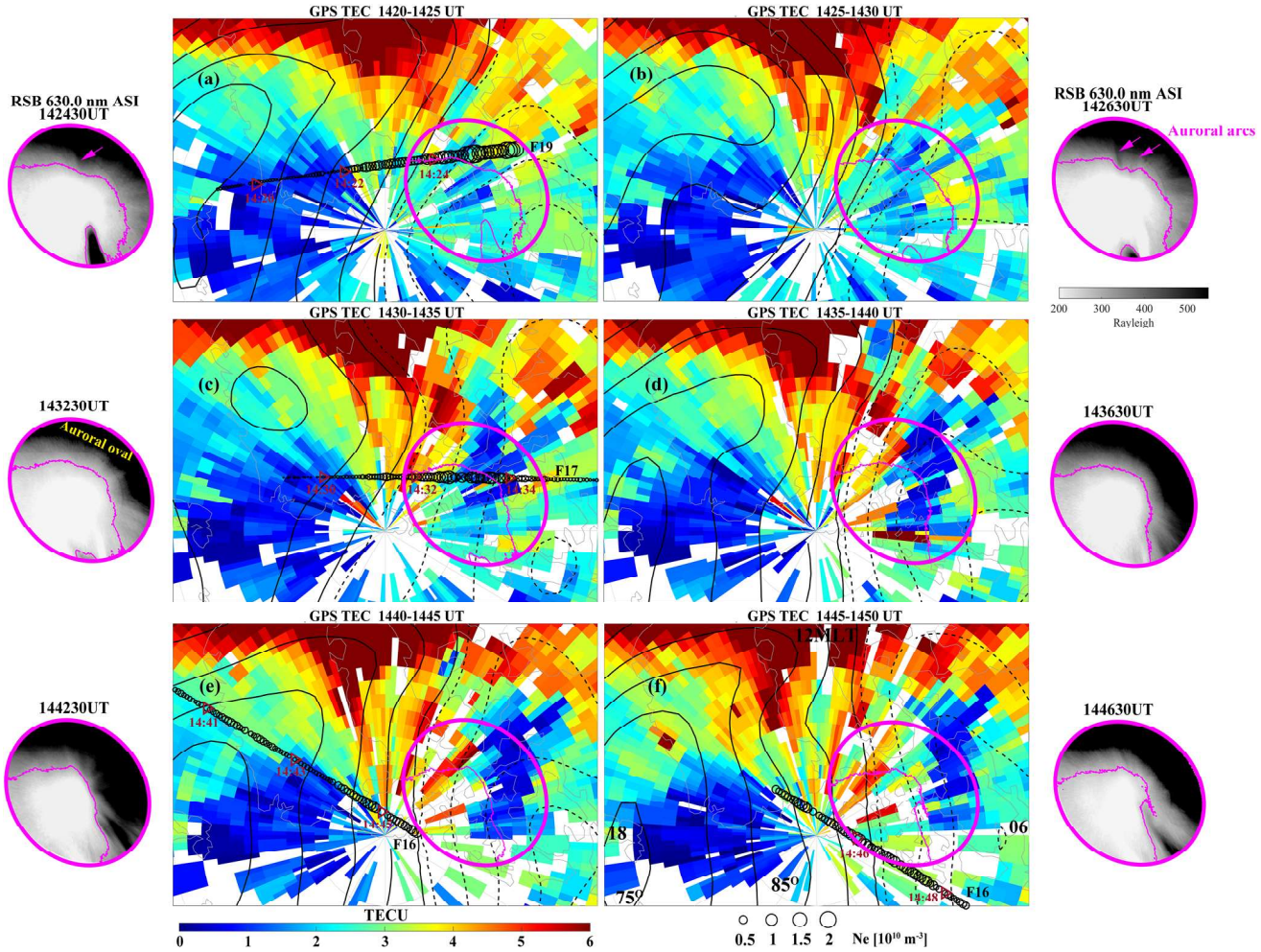

Figure 2. A series of GPS Total Electron Content maps, overlaid with Super Dual Auroral Radar Network convection patterns (the black dashed lines (solid lines) corresponding to the positive (negative) potential, interval 6 kV from ±1 kV), Resolute Bay (RSB) all-sky imager (ASI) 630.0 nm auroral emissions and the magnitude of the in situ Defense Meteorological Satellite Program (DMSP) electron densities plotted as circles. The dark red triangles highlight the location of the DMSP spacecraft at the specific times. The magenta lines in the RSB ASI observation are the contour lines corresponding to the 300 R intensity. Auroral oval and auroral arcs are highlighted with yellow markers and magenta arrows, respectively.

and the RSB ASI added high-resolution ground-based observation of the aurora. The DMSP SSUSI observation shows that there were multiple auroral arcs in the dawnside auroral oval.

Figure 2 shows the GPS TEC maps obtained from Madrigal database, overlaid by SuperDARN convection patterns (the black dashed lines (solid lines) corresponding to the positive (negative) potential, interval 6 kV from ±1 kV), RSB ASI 630.0 nm auroral emission, and the magnitude of the in situ DMSP satellite electron densities plotted as circles. Zenith angles less than 70° were used for the RSB ASI field-of-view. The dark red triangles highlight the location of the DMSP spacecraft at the specific times. The magenta lines in the RSB ASI observation are the contour lines corresponding to the 300 Rayleigh auroral boundary. The auroral oval and auroral arcs are highlighted with yellow markers and magenta arrows, respectively.

Figure 3a shows the trajectories of DMSP F16-F19 and Swarm A-C superimposed on top of the DMSP F17 SSUSI auroral observation around 1430–1436 UT. The cyan-blue lines mark the location of observed plasma density enhancements. There are three DMSP spacecraft crossings (F19, F17, and F16) that are relatively close in space and time and appear to capture the same patch event that drifted poleward in latitude from 78° to 81° magnetic latitude (MLAT). The orbit of the fourth spacecraft (F18) was a few minutes later and located further on the dayside and appears to capture a new polar cap patch event or the tail of this TOI/patch. Based on the GPS TEC maps, it seems more likely that it observed the tail of this TOI/patch. Figures 3b1–3b4 and 3c1–3c4 show the

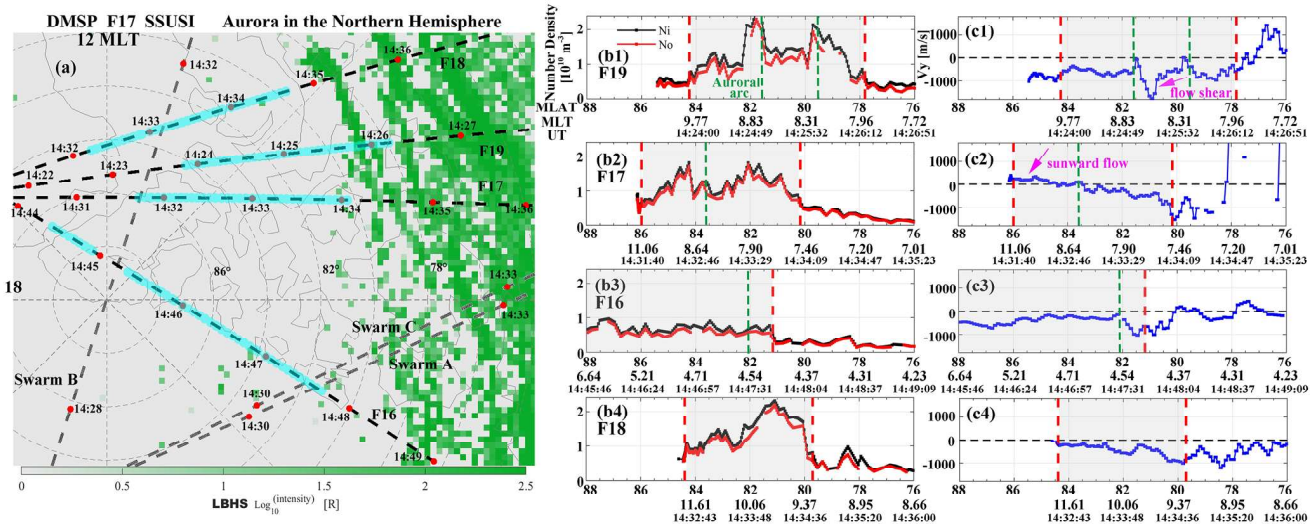

Figure 3. (a) The orbits of Defense Meteorological Satellite Program (DMSP) F16-F19 and Swarm A-C are superimposed on top of the DMSP F17 Special Sensor Ultraviolet Spectrographic auroral observation around 1430–1436 UT. The cyan-blue lines mark the location of plasma density enhancements. (b1-b4) The in situ ion and O^+ density and (c1-c4) cross-track ion drift velocity (Vy) observed by DMSP F16-F19. The vertical dashed red lines with shaded gray areas indicate the extent of the polar cap patches. The vertical dashed green lines highlight the location of enhanced auroral emission (arcs).

in situ ion and O^+ densities and cross-track ion drift velocities (Vy) versus MLAT, MLT and universal time (UT). The corresponding ion and electron temperatures and electron energy fluxes are shown in Figures 4a and 4b. Note that the F18 observation was not shown due to missing electron temperature data. The vertical dashed green lines in Figures 3b1–3b2, 3c1–3c2, 4a1–4a2, and 4b1–4b2 highlight the enhanced auroral emissions identified as arcs in Figure 2. DMSP F19 and F17 observed the dayside auroral arc structure mentioned earlier, and DMSP F16 saw another nightside auroral structure (vertical dashed green lines in Figures 3b3, 3c3, 4a3, and 4b3). The vertical dashed red lines with shaded gray areas indicate the extent of the polar cap patch. The polar cap patch was identified by the following steps: first, the polar cap boundaries in DMSP data were identified based on the method of Ma, Zhang, Xing, Jayachandran, et al. (2018) using high-energy particle precipitation flux cutoff (95% flux decreases) and the convection reversal; second, the background plasma densities were calculated by averaging the whole polar cap plasma densities; third, the areas with the plasma densities higher than the background were selected; fourth, the background plasma densities were recalculated by excluding the selected patch areas to eliminate the influence of patch densities on the background densities; fifth, selected patches were checked to see whether they had densities 2 times higher than the background densities. The selected patches must have 30 continuous data points (1s resolution) or 40 data points with small gaps to exclude the measurement perturbations. Note that we calculated the averaged plasma densities above 77° MLAT as the background plasma densities of Swarm data (the statistical auroral oval lies equatorward of the 77° MLAT) (Spicher et al., 2017). Other steps are consistent with those used to identify patches using DMSP data.

Combined with Figures 2–4, the evolution characteristics of the TOI/patch were analyzed as follows. There was a TOI that began to enter the polar cap from subauroral latitudes driven by the ionospheric convection pattern at about 1420 UT (Figure 2). DMSP F19 observed an increase in plasma density with double-peak accompanied by the flow shears as it passed through this region (Figures 3b1 and 3c1). At about 1424 UT the RSB ASI at 630.0 nm observed an auroral emission enhancement (Figure 2, ~350 Rayleigh, ~2 times higher than background) near the poleward boundary of the dawnside auroral oval [~9 MLT, ~82° MLAT] that continued to expand poleward, as shown by the magenta arrows in the 142,430 and 142,630 images. The auroral intensification is indicative of soft-electron precipitation. With the contribution of flow shears and particle precipitation, the plasma density distribution inside the TOI/patch was restructured, forming a wavy distribution (significant fluctuations with MLAT/MLT in DMSP F17-F19 plasma density observation in Figure 3).

Due to the continuous weakening of the emission intensity (displayed in black color scale and highlighted by magenta arrows in the Figure 2 and Movie S1), the auroral arcs were quite blurry when DMSP F17 crossed the polar region, but the double-peak density enhancement (Figure 3b2) and soft-electron precipitation (Figure 4b2)

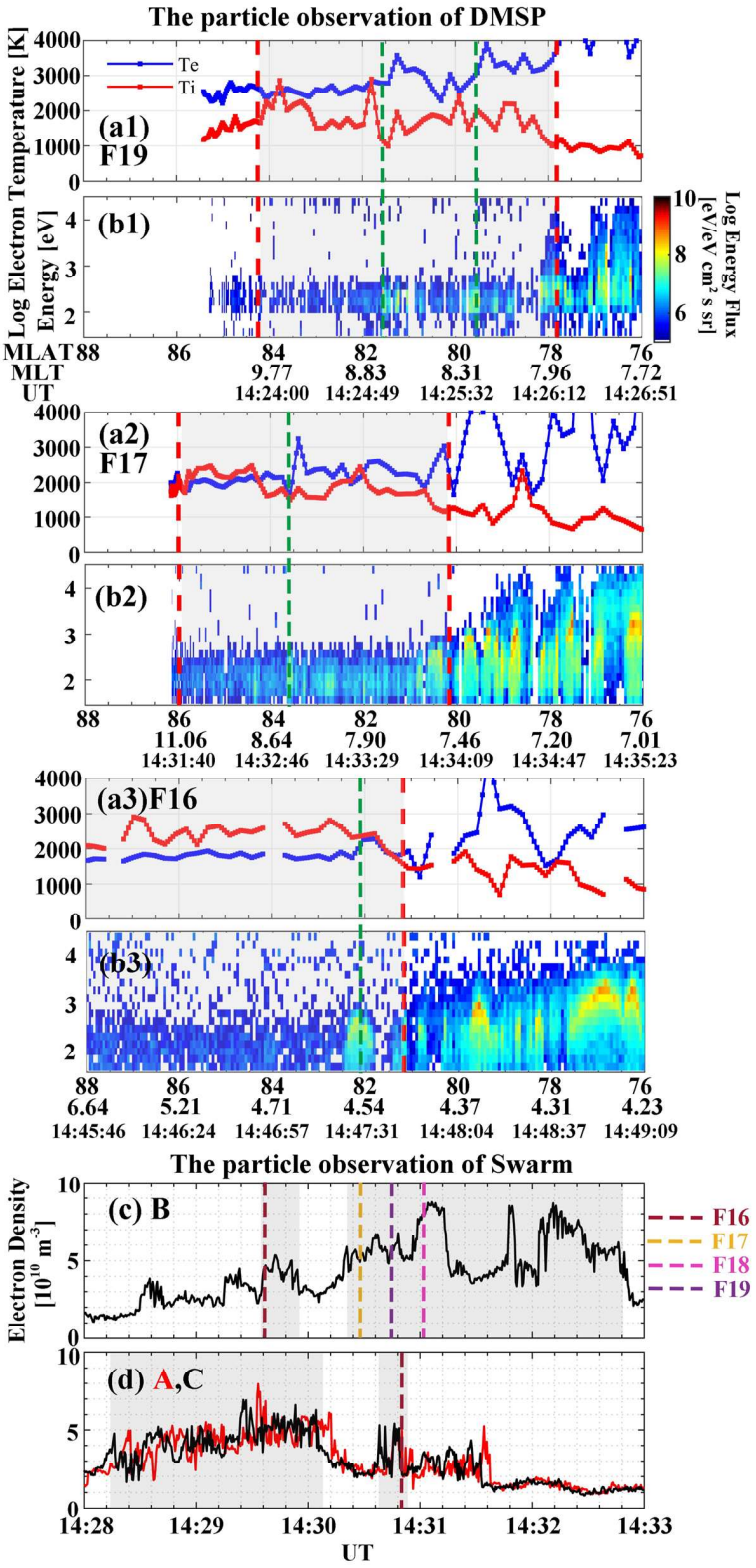

Figure 4. (a1–a4) The ion and electron temperature and (b1–b4) electron energy flux observed by Defense Meteorological Satellite Program (DMSP) F19, F17 and F16. The vertical dashed red lines with shaded gray areas have the same meaning as in Figures 3b and 3c. The vertical dashed green lines highlight the enhanced auroral emission (arcs). The in situ electron density observed by (c) Swarm-B, and (d) Swarm A and C. The vertical dashed lines indicate the times when the Swarm tracks intersected the DMSP tracks.

were still observed. The DMSP F17 soft-electron precipitation occurred over a wider range and has a lower energy flux peak occurred at a lower energy (Figure 4b2). Moreover, the F17 sunward flow was observed on the higher latitude side of the patch (Figures 3 and 4). Around 1430 UT the poleward boundary of the dawn-side auroral oval (~6–8 MLT) moved to higher latitudes, which gave a dawn-dusk shift of the patch. This is consistent with F16 and F17 observing the patch to be closer to the polar cap center than for F19 a few minutes earlier. Note that the DMSP F18 orbit is not shown because the electron density observation from that spacecraft is unavailable. DMSP F19 observed the patch around 1425 UT, and the electron temperature of the patch was about 1,000 K higher than the ion temperature, which is called a "hot patch" (Zhang et al., 2017; Ma, Zhang, Xing, Heelis, et al., 2018; D. Zhang et al., 2021, 2022). The plasma density of the hot patch had double-peak of about $2*10^{10}$ m^{-3} associated with the soft-electron precipitation. Between these density peaks there was a strong anti-sunward flow of about 1,800 m/s, which matches the density depletion in the patch center. After 8 min, F17 and F18 crossed the polar region. The F18 track was closer to the dayside, and F17 was closer to the nightside in the dawnside polar region. DMSP F17, F18 and F19 all have similar density double-peak structures. Combined with the GPS TEC maps, they all passed through the same total electron content units (TECU) enhanced structure as it extended deep into the polar cap. The maximum patch density of F17 was approximately $1.6*10^{10}$ m^{-3} with some soft-electron precipitation. The higher latitude side of the patch showed cold patch characteristics (Te ~2,000 K, Ti ~2,000 K) with sunward flow, and the lower latitude side showed hot patch characteristics (Te ~2,300 K, Ti ~1,700 K) with anti-sunward flow. Notice that there is a difference between the convection patterns observed by DMSP and SuperDARN, because SuperDARN uses filtered data (2 min time average, median filtering, and fitting to a statistical convection model), while DMSP shows actual in situ variations along the satellite track. Consequently, the local sunward flow on the high-latitude side of the patch may bring low-density plasma from the nightside to accelerate the decreasing patch density. The lower latitude side of the patch still had high electron temperature, which was related to soft-electron precipitation. F16 observed the patch at about 1446 UT, and the plasma density of the patch was ~$0.7*10^{10}$ m^{-3}. The patch then exhibited cold patch characteristics with only very weak soft-electron precipitation.

Figures 4c and 4d show the in situ electron densities observed by (c) Swarm B, and (d) Swarm A and C. The vertical dashed lines highlight the times when the Swarm tracks intersected the DMSP tracks. The gray shadings highlight the extent of the polar cap patches. The plasma density was always high when Swarm-B passed through the area. This suggests that Swarm B passed through the patch (shaded gray area) in the day-night direction, and the plasma density of the patch was lower closer to the nightside. The plasma density at ~500 km was at least 4 times higher than at ~800 km, while the electron temperature and the field-aligned current measurements only had small perturbations (not shown).

4. Discussion

In this work, six satellites crossed a TOI/patch within ~20-min as it moved from the dayside to the nightside. It was initially hot, before it changed to a mix of cold and hot, and finally it became a cold patch. Several different instruments observed the same event: (a) The TECU enhancement traveled from the dayside to the magnetic pole according to TEC maps (Figure 2). There was a TOI entering the polar cap from subauroral latitudes, that subsequently turned into a polar cap patch. The DMSP satellites all observed density enhancements when passing through the structure. Note that it is difficult to give the accurate movement in the nightside sector due to missing TEC data. (b) The anti-sunward horizontal velocity observed by F19 was about 650 m/s. Assuming the patch traveled at a constant velocity, it moved about 300 km (3° MLAT) in 8 min, and about 800 km (8° MLAT) in 22 min toward the nightside. The distance between the DMSP satellite tracks corresponded to the distance traveled by the patch; (c) The in situ electron density was continuously high when Swarm B crossed the F17 and F19 tracks. It was identified as a single polar cap patch according to the patch criterion; (d) the ASI observed the clearly enhanced auroral emission (aurora arcs) at the polar cap boundary [~9 MLT, ~82° MLAT] around 1424 UT. After 2 min, the auroral intensity increased, and the enhanced emission intensities correspond to the positions of the density enhancements observed by DMSP F19. Then, the enhanced auroral emission moved toward the polar cap, and decreased continuously (Figure 2, Movie S1). Around 1432 UT, DMSP F17 still detected a density enhancement and soft-electron precipitation near the area where the arc became blurred, indicating that its influence still existed (Movie S1). In summary, DMSP F16, F17 and F19 observed the same TOI/patch and the orbit of DMSP F18 was a few minutes later and located further on the dayside and appears to capture a new polar cap patch event or the tail of this TOI/patch.

The event showed the characteristics of a hot patch when it was observed by F19. Combined with observations from the RSB ASI, the location of the patch was close to the dayside auroral oval, and it was accompanied by soft-electron precipitation, which resulted in the higher electron temperature. An area of sunward flow was observed by DMSP F17 on the higher latitude side of the patch (close to the polar cap center), resulting in flow shears. The cold plasma was transported from the nightside toward the dayside. As the polar cap patch evolved further toward the nightside, the soft-electron precipitation disappeared, there was no heat source, and the electron temperature decreased rapidly. The patch was finally characterized as a cold patch. For the event, both IMF By and Bz were very close to zero, and negative radial IMF Bx was the dominant component. The ionospheric convection pattern was weaker than under strong southward IMF Bz conditions. Consequently, it takes longer time before a patch makes it across the polar cap and to the nightside. On this basis, strong radial negative IMF Bx resulted in lobe reconnection in the northern hemisphere (Wang et al., 2022), which may drive the formation of the flow shears in the polar cap. It is consistent with the DMSP SSIES data, but SuperDARN does not capture it very well, likely because none of the SuperDARN convection models that are used for fitting are tailored for such a peculiar IMF orientation of dominant IMF Bx. SuperDARN convection models typically only fit against IMF Bz and By.

To explore the effect of soft-electron precipitation on the electron temperature of the patch, the correlation coefficients (R) between soft-electron energy flux and electron temperature are calculated. The correlation coefficient of the patch was about 0.37 for F19, 0.41 for F17, and 0.32 for F16. It suggests that soft-electron precipitation plays a key role for the electron temperature variation of the patch. Su et al. (1999) also found that the electron temperature increased with enhanced auroral soft-electron precipitation. Moreover, the evolution process indicates that the cold patch is not only caused by the dayside high-density plasma produced by solar EUV radiation, but a cold patch may also appear when a hot patch cools down. The cold patch produced by this latter process may be located more toward the nightside polar cap, because it takes time to cool down a hot patch. More research is needed to parameterize such events (such as, how long does it take to cool down?), and most of the scientific literature has been focusing on plasma patches during southward IMF, and not radial IMF that we are reporting on here.

The peak density of the polar cap patch was given in the observation section. Because it is not straightforward to inter-calibrate the in situ plasma density measurements of multiple spacecrafts, we only look at changes in the relative plasma density (plasma density vs. background calculated for each spacecraft). The mean density of the patch was 6.6 times (patch: $1.31*10^{10}$ m^{-3}; background: $0.20*10^{10}$ m^{-3}) higher than the background for F19, decreased to 5.1 times (patch: $1.02*10^{10}$ m^{-3}; background: $0.20*10^{10}$ m^{-3}) for F17, and finally only 2.6 times (patch: $0.63*10^{10}$ m^{-3}; background: $0.24*10^{10}$ m^{-3}) for F16. This may be due to enhanced plasma recombination associated with enhanced flow shears (strong anti-sunward flow observed by F19 and sunward flow observed by F17) leading to frictional ion heating (e.g., Schunk et al., 1975; Zettergren & Semeter, 2012; Zhang et al., 2016). However, the process is highly efficient at altitudes of 200–300 km and less effective in the topside ionosphere. The sunward transport of cold plasma close to the nightside polar cap should also be considered. The patch density observed by F19 had double-peak structure, corresponding to the strongest auroral emission of the dayside aurora, and a valley in between that corresponded to strong anti-sunward flow (~1,800 m/s). The associated intense flow shears may result in plasma depletion (Scales et al., 1995). Moreover, as the patch evolved toward the nightside, it gradually moved away from its high-density plasma source (plasma production ended) meaning decreased production. As the patch traveled from the dayside to the nightside, it also experienced a small shift in the dawn-dusk direction. Figure 2 and Movie S1 show that the dawnside auroral oval contracted toward higher latitudes about 1432 UT, implying that the open-closed field line boundary drifted poleward. SuperDARN observations (Figure S1 in Supporting Information S1) suggest a contraction of the equatorward ionospheric convection boundary.

An auroral structure was observed by the RSB ASI at 1424 UT near 9 MLT, and it extended poleward into the polar cap. The enhanced plasma density associated with this structure was monitored by the DMSP satellites, and the polar cap patch was associated with red line emission intensity enhancement, which may be due to increased O^+ concentration and decreased O_2 concentration (Coley & Heelis, 1995). Consequently, the polar cap patch had identifiable features at different heights spanning from ~200 to ~800 km. There were also several auroral arcs on the nightside from 1404 UT observed by the RSB ASI at 630.0 nm band. Previous studies have suggested that polar cap patches are related to dayside auroral structures like poleward moving auroral form (PMAF) (Lorentzen et al., 2010; Nishimura et al., 2014; Zhang et al., 2010) and throat aurora (Zhang et al., 2023). Our auroral arc

was accompanied by electron density enhancement and soft-electron precipitation (Michell et al., 2008), but the relationships between polar cap patches and auroral arcs in the polar cap needs to be investigated in future work.

5. Conclusion

We have presented simultaneous observations from multiple DMSP and Swarm satellites, an ASI at RSB, and SuperDARN to investigate the evolution and key characteristics of a high-density TOI/patch. Six satellites crossed the polar cap TOI/patch as it traveled from the dayside to the nightside, which provided unprecedented information on its temporal and spatial evolution. The event started out as hot plasma, before it became a mix of hot and cold, and finally it became a cold patch. Both soft-electron precipitation and flow shears contributed to its evolution. It suggests that a cold patch is not only caused by solar EUV radiation, but can also be the result of a hot patch cooling down. The patch density at ~500 km was at least 4 times higher than at ~800 km. The electron density gradually decreased as the polar cap patch traveled toward to the nightside, due to decreased plasma production and transport of cold nightside low-density plasma. The patch's motion was influenced by changes in the ionospheric convection pattern.

Data Availability Statement

CEDAR Madrigal and JHU/APL have provided the DMSP in situ particle data (http://cedar.openmadrigal.org/list/, registering personal information and choosing "Defense meteorological satellite Program") and SSUSI auroral emission data (https://ssusi.jhuapl.edu/data_products, choosing "Auroral EDR"). CEDAR Madrigal also has provided the TEC map data. The European Space Agency (ESA) has provided the Swarm satellites data (https://earth.esa.int/eogateway/catalog). The NASA OMNI database (http://omniweb.gsfc.nasa.gov) provides the IMF data. We acknowledge the use of SuperDARN data, and the data during 14–15 UT on 12 December 2015 is stored in https://doi.org/10.5281/zenodo.10003810. SuperDARN is a network of radars funded by national scientific funding agencies of Australia, Canada, China, France, Italy, Japan, Norway, South Africa, the United Kingdom, and the United States of America. The RSB ASI data at 630.0 nm is obtained from https://ergsc.isee.nagoya-u.ac.jp/data/ergsc/ground/camera/omti/asi/rsb/2015/12/12/.

Acknowledgments
The work in China was supported by the National Natural Science Foundation of China (Grants 42325404, 42120104003, 41874170, 41831072, and 42204164), the Chinese Meridian Project, the China Postdoctoral Science Foundation (Grant 2021M701974), the International Partnership Program of Chinese Academy of Sciences (Grant 183311KYSB20200003), Shandong Provincial Natural Science Foundation (Grant ZR2022QD077) and China Scholarship Council (Grant 202206220115). Work at UCLA has been supported by NSF grant AGS-2055192. This research was supported by the International Space Science Institute (ISSI) in Bern and Beijing, through ISSI International Team project #511 (Multi-Scale Magnetosphere-Ionosphere-Thermosphere Interaction). The authors acknowledge the use of SuperDARN data. SuperDARN is a collection of radars funded by national scientific funding agencies of Australia, Canada, China, France, Italy, Japan, Norway, South Africa, United Kingdom, and the United States of America.

References

Aarons, J. (1982). Global morphology of ionospheric scintillation. *Proceedings of the IEEE*, *70*(4), 360–378. https://doi.org/10.1109/PROC.1982.12314

Basu, S., MacKenzie, E., Costa, E., Fougere, P., Carlson, H., & Whitney, H. (1987). 250 MHz/GHz scintillation parameters in the equatorial, polar, and auroral environments. *IEEE Journal on Selected Areas in Communications*, *5*(2), 102–115. https://doi.org/10.1109/JSAC.1987.1146533

Buchert, S., Zangerl, F., Sust, M., André, M., Eriksson, A., Wahlund, J., & Opgenoorth, H. (2015). SWARM observations of equatorial electron densities and topside GPS track losses. *Geophysical Research Letters*, *42*(7), 2088–2092. https://doi.org/10.1002/2015GL063121

Carlson, H. C., Oksavik, K., Moen, J., & Pedersen, T. (2004). Ionospheric patch formation: Direct measurements of the origin of a polar cap patch. *Geophysical Research Letters*, *31*(8), L08806. https://doi.org/10.1029/2003GL018166

Chisham, G., Lester, M., Milan, S. E., Freeman, M. P., Bristow, W. A., Grocott, A., et al. (2007). A decade of the super dual auroral radar network (SuperDARN): Scientific achievements, new techniques and future directions. *Surveys in Geophysics*, *28*(1), 33–109. https://doi.org/10.1007/s10712-007-9017-8

Coley, W. R., & Heelis, R. A. (1995). Adaptive identification and characterization of polar ionization patches. *Journal of Geophysical Research*, *100*(A12), 23819–23827. https://doi.org/10.1029/95JA02700

Crowley, G. (1996). A critical review of ionospheric patches and blobs. In *Review of radio science 1993–1996* (pp. 619–648). Oxford University Press.

Dungey, W. J. (1961). The steady state of the Chapman-Ferraro problem in two dimensions. *Journal of Geophysical Research*, *66*(4), 1043–1047. https://doi.org/10.1029/jz066i004p01043

Goodwin, L. V., Iserhienrhien, B., Miles, D. M., Patra, S., van der Meeren, C., Buchert, S. C., et al. (2015). Swarm in situ observations of F region polar cap patches created by cusp precipitation. *Geophysical Research Letters*, *42*(4), 996–1003. https://doi.org/10.1002/2014GL062610

Greenspan, M. E., Anderson, P. B., & Pelagatti, J. M. (1986). *Characteristics of the thermal plasma monitor (SSIES) for the Defense meteorological satellite Program (DMSP) spacecraft S8 through F10* Tech. Rep. AFGL- TR-86- 0227. Hanscom AFB.

Hardy, D. A., Holeman, E. G., Burke, W. J., Gentile, L. C., & Bounar, K. H. (2008). Probability distributions of electron precipitation at high magnetic latitudes. *Journal of Geophysical Research*, *113*(A6), A06305. https://doi.org/10.1029/2007JA012746

Kivanç, O., & Heelis, R. A. (1997). Structure in ionospheric number density and velocity associated with polar cap ionization patches. *Journal of Geophysical Research*, *102*(A1), 307–318. https://doi.org/10.1029/96ja03141

Liou, K., Newell, P. T., Meng, C.-I., Brittnacher, M., & Parks, G. (1998). Characteristics of the solar wind controlled auroral emissions. *Journal of Geophysical Research*, *103*(A8), 17543–17557. https://doi.org/10.1029/98JA01388

Lockwood, M., & Carlson, H. C. (1992). Production of polar cap electron density patches by transient magnetopause reconnection. *Geophysical Research Letters*, *19*(17), 1731–1734. https://doi.org/10.1029/92GL01993

Lorentzen, D. A., Moen, J., Oksavik, K., Sigernes, F., Saito, Y., & Johnsen, M. G. (2010). In situ measurement of a newly created polar cap patch. *Journal of Geophysical Research*, *115*(A12), A12323. https://doi.org/10.1029/2010JA015710

Ma, Y.-Z., Zhang, Q.-H., Lyons, L., Oksavik, K., Xing, Z.-Y., Hairston, M., et al. (2023). A comparative study on the hot dense plasma and cold patch by using multi-instrument observations. *Journal of Geophysical Research: Space Physics*, *128*(6), e2022JA031166. https://doi.org/10.1029/2022JA031166

Ma, Y.-Z., Zhang, Q.-H., Xing, Z.-Y., Heelis, R. A., Oksavik, K., & Wang, Y. (2018). The ion/electron temperature characteristics of polar cap classical and hot patches and their influence on ion upflow. *Geophysical Research Letters*, *45*(6), 8072–8080. https://doi.org/10.1029/2018GL079099

Ma, Y.-Z., Zhang, Q.-H., Xing, Z.-Y., Jayachandran, P. T., Moen, J., Heelis, R. A., & Wang, Y. (2018b). Combined contribution of solar illumination, solar activity, and convection to ion upflow above the polar cap. *Journal of Geophysical Research: Space Physics*, *123*(5), 4317–4328. https://doi.org/10.1029/2017JA024974

Michell, R. G., Lynch, K. A., Heinselman, C. J., & Stenbaek-Nielsen, H. C. (2008). PFISR nightside observations of naturally enhanced ion acoustic lines, and their relation to boundary auroral features. *Annales Geophysicae*, *26*(11), 3623–3639. https://doi.org/10.5194/angeo-26-3623-2008

Mitchell, C. N., Alfonsi, L., De Franceschi, G., Lester, M., Romano, V., & Wernik, A. W. (2005). GPS TEC and scintillation measurements from the polar ionosphere during the October 2003 storm. *Geophysical Research Letters*, *32*(12), L12S03. https://doi.org/10.1029/2004GL021644

Moen, J., Oksavik, K., Alfonsi, L., Daabakk, Y., Romano, V., & Spogli, L. (2013). Space weather challenges of the polar cap ionosphere. *Journal of Space Weather and Space Climate*, *3*, A02. https://doi.org/10.1051/SWSC/2013025

Moen, J., Qiu, X. C., Carlson, H. C., Fujii, R., & McCrea, I. W. (2008). On the diurnal variability in F2-region plasma density above the EISCAT Svalbard radar. *Annales Geophysicae*, *26*(8), 2427–2433. https://doi.org/10.5194/angeo-26-2427-2008

Nishimura, Y., Lyons, L. R., Zou, Y., Oksavik, K., Moen, J. I., Clausen, L. B., et al. (2014). Day-night coupling by a localized flow channel visualized by polar cap patch propagation. *Geophysical Research Letters*, *41*(11), 3701–3709. https://doi.org/10.1002/2014GL060301

Nishimura, Y., Sadler, F. B., Varney, R. H., Gilles, R., Zhang, S. R., Coster, A. J., et al. (2021). Cusp dynamics and polar cap patch formation associated with a small IMF southward turning. *Journal of Geophysical Research: Space Physics*, *126*(5), e2020JA029090. https://doi.org/10.1029/2020JA029090

Oksavik, K., Barth, V. L., Moen, J., & Leste, M. (2010). On the entry and transit of high-density plasma across the polar cap. *Journal of Geophysical Research*, *115*(A12), A12308. https://doi.org/10.1029/2010JA015817

Paxton, L. J., Meng, C. I., Fountain, G. H., Ogorzalek, B. S., Darlington, E. H., Goldstein, J., et al. (1992). Special sensor UV spectrographic imager (SSUSI): An instrument description. *Instrumentation for Planetary and Terrestrial Atmospheric Remote Sensing*, *1745*, 2–15.

Ren, J., Zou, S., Gillies, R. G., Donovan, E., & Varney, R. H. (2018). Statistical characteristics of polar cap patches observed by RISR-C. *Journal of Geophysical Research: Space Physics*, *123*(8), 6981–6995. https://doi.org/10.1029/2018JA025621

Scales, W., Bernhardt, P., & Ganguli, G. (1995). Early time evolution of a chemically produced electron depletion. *Journal of Geophysical Research*, *100*(A1), 269–280. https://doi.org/10.1029/94JA02490

Schunk, R. W., Raitt, W. J., & Banks, P. M. (1975). Effect of electric fields on the daytime high-latitude E and F regions. *Journal of Geophysical Research*, *80*(22), 3121–3130. https://doi.org/10.1029/JA080i022p03121

Shiokawa, K., Katoh, Y., Satoh, M., Ejiri, M. K., Ogawa, T., Nakamura, T., et al. (1999). Development of optical mesosphere thermosphere imager (OMTI). *Earth Planets and Space*, *51*(7–8), 887–896. https://doi.org/10.1186/BF03353247

Shiokawa, K., Otsuka, Y., & Ogawa, T. (2009). Propagation characteristics of nighttime mesospheric and thermospheric waves observed by optical mesosphere thermosphere imagers at middle and low latitudes. *Earth Planets and Space*, *61*(4), 479–491. https://doi.org/10.1186/BF03353165

Spicher, A., Clausen, L. B. N., Miloch, W. J., Lofstad, V., Jin, Y., & Moen, J. I. (2017). Interhemispheric study of polar cap patch occurrence based on Swarm in situ data. *Journal of Geophysical Research: Space Physics*, *122*(3), 3837–3851. https://doi.org/10.1002/2016JA023750

Su, Y.-J., Caton, R. G., Horwitz, J. L., & Richards, P. G. (1999). Systematic modelling of soft-electron precipitation effects on high-latitude F region and topside ionospheric upflows. *Journal of Geophysical Research*, *104*(A1), 153–163. https://doi.org/10.1029/1998JA900068

Wang, Z., Lu, J., Hu, H., Liu, J., Hu, Z., Wang, M., et al. (2022). HMB variations measured by SuperDARN during the extremely radial IMFs: Is the coupling function applicable in radial IMF? *Journal of Geophysical Research: Space Physics*, *127*(2), e2021JA029589. https://doi.org/10.1029/2021ja029589

Xing, Z. Y., Yang, H. G., Han, D. S., Wu, Z. S., Hu, Z. J., Zhang, Q. H., et al. (2012). Poleward moving auroral forms (PMAFs) observed at the Yellow River station: A statistical study of its dependence on the solar wind conditions. *Journal of Atmospheric and Solar-Terrestrial Physics*, *86*, 25–33. https://doi.org/10.1016/j.jastp.2012.06.004

Zettergren, M., & Semeter, J. (2012). Ionospheric plasma transport and loss in auroral downward current regions. *Journal of Geophysical Research*, *117*(A6), A06306. https://doi.org/10.1029/2012JA017637

Zhang, D., Zhang, Q.-H., Ma, Y.-Z., Oksavik, K., Lyons, L. R., Xing, Z.-Y., et al. (2022). The dependence of cold and hot patches on local plasma transport and particle precipitation in Northern Hemisphere winter. *Geophysical Research Letters*, *49*(12), e2022GL098671. https://doi.org/10.1029/2022GL098671

Zhang, D., Zhang, Q.-H., Ma, Y.-Z., Oksavik, K., Lyons, L. R., Zhang, Y.-L., et al. (2021). Solar and geomagnetic activity impact on occurrence and spatial size of cold and hot polar cap patches. *Geophysical Research Letters*, *48*(18), e2021GL094526. https://doi.org/10.1029/2021GL094526

Zhang, D., Zhang, Q.-H., Oksavik, K., Xu, T., Xing, Z.-Y., Lyons, L. R., et al. (2023). Do the throat auroras create polar cap patches? *Geophysical Research Letters*, *50*(7), e2022GL102263. https://doi.org/10.1029/2022GL102263

Zhang, Q.-H., Dunlop, M. W., Lockwood, M., Liu, R.-Y., Hu, H.-Q., Yang, H.-G., et al. (2010). Simultaneous observations of reconnection pulses at Cluster and their effects on the cusp aurora observed at the Chinese Yellow River Station. *Journal of Geophysical Research*, *115*(A10), A10237. https://doi.org/10.1029/2010JA015526

Zhang, Q.-H., Lockwood, M., Foster, J. C., Zhang, S.-R., Zhang, B.-C., McCrea, I. W., et al. (2015). Direct observations of the full Dungey convection cycle in the polar ionosphere for southward interplanetary magnetic field condition. *Journal of Geophysical Research: Space Physics*, *120*(6), 4519–4530. https://doi.org/10.1002/2015JA021172

Zhang, Q.-H., Ma, Y.-Z., Jayachandran, P. T., Moen, J., Lockwood, M., Zhang, Y.-L., et al. (2017). Polar cap hot patches: Enhanced density structures different from the classical patches in the ionosphere. *Geophysical Research Letters*, *44*(16), 8159–8167. https://doi.org/10.1002/2017GL073439

Zhang, Q.-H., Moen, J. I., Lockwood, M., McCrea, I., Zhang, B.-C., McWilliams, K. A., et al. (2016). Polar cap patch transportation beyond the classic scenario. *Journal of Geophysical Research: Space Physics*, *121*(9), 9063–9074. https://doi.org/10.1002/2016JA022443

Zhang, Q.-H., Xing, Z.-Y., Wang, Y., & Ma, Y.-Z. (2020). Formation and evolution of polar cap ionospheric patches and their associated upflows and scintillations: A review. In Q. G. Zong, P. Escoubet, D. Sibeck, G. Le, & H. Zhang (Eds.), *Dayside magnetosphere interaction* (pp. 286–302). John Wiley & Sons, Inc. https://doi.org/10.1002/9781119509592.ch16

Zhang, Q.-H., Zhang, B.-C., Hu, H.-Q., Moen, J., Lockwood, M., Yang, H. G., et al. (2013). Polar cap patch segmentation of the tongue of ionization in the morning convection cell. *Geophysical Research Letters*, *40*(12), 2918–2922. https://doi.org/10.1002/grl.50616

Zhang, Q.-H., Zhang, B.-C., Liu, R.-Y., Dunlop, M. W., Lockwood, M., Moen, J., et al. (2011). On the importance of IMF |BY| on polar cap patch formation. *Journal of Geophysical Research*, *116*(A5), A05308. https://doi.org/10.1029/2010JA016287

Zhang, Q.-H., Zhang, B.-C., Lockwood, M., Hu, H.-Q., Moen, J. I., Ruohoniemi, J. M., et al. (2013). Direct observations of the evolution of polar cap ionization patches. *Science*, *339*(6127), 1597–1600. https://doi.org/10.1126/science.1231487